Check for updates

Synthesis of novel naphthalene-heterocycle hybrids with potent antitumor, anti-inflammatory and antituberculosis activities†

Mohamed Ahmed Abozeid, [ID]ᵃ Aya Atef El-Sawi,ᵃ Mohamed Abdelmoteleb, [ID]ᵇᶜ Hanem Awad, [ID]ᵈ Marwa Mostafa Abdel-Aziz,ᵉ Abdel-Rahman Hassan Abdel-Rahmanᵃ and El-Sayed Ibrahim El-Desoky [ID] *ᵃ

Multitarget-directed drugs (hybrid drugs) constitute an efficient avenue for the treatment of multifactorial diseases. In this work, novel naphthalene hybrids with different heterocyclic scaffolds such as nicotinonitrile, pyran, pyranopyrazole, pyrazole, pyrazolopyridine, and azepine were efficiently synthesized *via* tandem reactions of 3-formyl-4*H*-benzo[*h*]chromen-4-one **1** with different nucleophilic reagents. Analysis of these hybrids using PASS online software indicated different predicted biological activities such as anticancer, antimicrobial, antiviral, antiprotozoal, anti-inflammatory, *etc.* By focusing on antitumor, anti-inflammatory, and antituberculosis activities, many compounds revealed remarkable activities. While **3c**, **3e**, and **3h** were more potent than doxorubicin in the case of HepG-2 cell lines, **3a**–**e**, **3i**, **6**, **8**, **10**, **11**, and **12b** were more potent in the case of MCF-7. Moreover, compounds **3c**, **3h**, **8**, **10**, **3d**, and **12b** manifested superior activity and COX-2 selectivity to the reference anti-inflammatory Celecoxib. Regarding antituberculosis activity, **3c**, **3d**, and **3i** were found to be the most promising with MIC less than 1 μg mL^{-1}. The molecular docking studies showed strong polar and hydrophobic interactions with the novel naphthalene-heterocycle hybrids that were compatible with experimental evaluations to a great extent.

Introduction

Naphthalene constitutes a flexible and multifaceted platform in medicinal chemistry.[1] This scaffold emerges as a promising moiety in drug design due to its diverse biological activities generated from structural modifications. Various antagonistic activities were reported for naphthalene-based compounds such as antimicrobial,[2] anticancer,[3] antiviral,[4] anticonvulsant,[5] antitubercular,[6] and anti-inflammatory.[7] Besides, different naturally occurring compounds including the naphthalene nucleus revealed notable biological activities such as justicidin

A (anticancer),[8] rifampicin (antitubercular),[9] patentiflorin A (anti-HIV),[10] and bis-ANS 82 (tubulin polymerization inhibitor).[11] In 2018, Kittakoop and his team isolated a set of naphthalene derivatives from *Ventilago denticulata* which exhibited promising antibacterial and cytotoxic activities in addition to aromatase and phosphodiesterase inhibitory activities.[12] Naphthalene nucleus also appeared in different marketed therapeutics such as Nafcillin,[13] Bedaquiline,[14] Naproxen,[15] and Nafimidone[16] (Fig. 1).

Moreover, naphthalene was known to be metabolized intracellularly into naphthoquinone and naphthalene epoxide that could react with thiol group (SH) of cysteine amino acid residue *via* nucleophilic substitution and 1,4-Michael addition, respectively.[17] 1-Naphthol and naphthoquinone were also reported to produce reactive oxygen species (ROS) under the effect
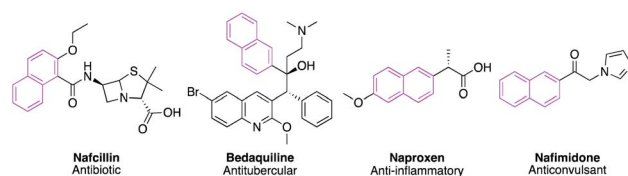
ᵃ*Department of Chemistry, Faculty of Science, Mansoura University, Mansoura-35516, Egypt. E-mail: prof.deosky.orgchem@gmail.com; desoky199@mans.edu.eg; Tel: +201060614054*

ᵇ*Food Allergy Research & Resource Program (FARRP), Department of Food Science & Technology, University of Nebraska, Lincoln, NE, USA*

ᶜ*Department of Botany, Faculty of Science, Mansoura University, Mansoura-35516, Egypt*

ᵈ*Department of Tanning Materials and Leather Technology, Chemical Industries Research Division, National Research Centre, 33 EL-Bohouth St., Dokki 12622, Giza, Egypt*

ᵉ*The Regional Center for Mycology and Biotechnology, Al-Azhar University, Cairo 11759, Egypt*

† Electronic supplementary information (ESI) available. See DOI: 10.1039/d0ra08526j

Fig. 1 Representative examples for naphthalene containing marketed drugs.

of hepatic microsomal enzymes[18] that recently achieved promising results in cancer treatment.[19] Additionally, naphthoquinone fulfilled Lipinski's rule of five to be an orally active drug.

On the other hand, multitarget-directed compounds are the combination of two or more distinctive biologically active molecules into one entity to achieve dual-drug action.[20] This hybrid design would be promising to treat multifactorial diseases such as cancer in addition to neurodegenerative disorders including Parkinson's and Alzheimer's disease. The drug hybridization could also generate new molecules with lower toxicity, improved affinity, and better pharmacokinetics in addition to avoiding common drug–drug interactions observed in drug cocktails.[20] As seen in Fig. 1 examples, naphthalene could form very efficient hybrid drugs by merging with different biologically active moieties. Moreover, our previous studies unveiled different promising hybrid molecules that resulted from the combination of naphthalene with pyran, pyridine, pyrazole, and others.[2]

Herein, new naphthalene hybrids with nicotinonitrile, pyrazole, and pyran moieties were designed (Fig. 2). Moreover, molecular hybridization of naphthalene with pyrazolopyridine[21] and azepine[22] pharmacophores was reported for the first time (Fig. 2). The anticancer, anti-inflammatory, and antituberculosis activities of the synthesized compounds were evaluated, and the results were analyzed in light of the molecular docking.

Results and discussion

Chemistry

The Knoevenagel condensation of formylchromone 1[23] with different cyanoacetanilide derivatives $2a–h$[24] as 1,3-C,N-dinucleophiles in the presence of a catalytic amount of triethylamine afforded the corresponding nicotinonitrile derivatives $3a–h$ in excellent yields (Scheme 1). First, carbon nucleophilic center, which was generated from cyanoacetanilides $2a–h$ by deprotonation under basic conditions, attacked the formyl group followed by dehydration to give intermediate $1A$. After that, NH functionality underwent conjugate addition to α,β-unsaturated carbonyl moiety of chromone nucleus to give intermediate $1B$. The ring-opening of chromene intermediate $1B$ generated nicotinonitrile derivatives $3a–h$. Similarly, the condensation of formylchromone 1 with 2-cyano-N'-(1-(2-oxo-2H-chromen-3-yl)-ethylidene)acetohydrazide (4)[25] afforded multi-functionalized derivative $3i$ (Scheme 1).
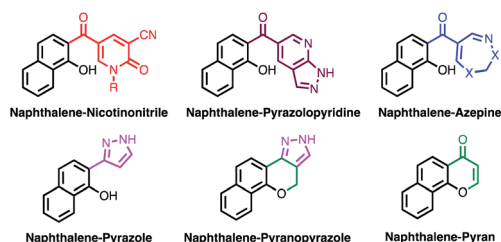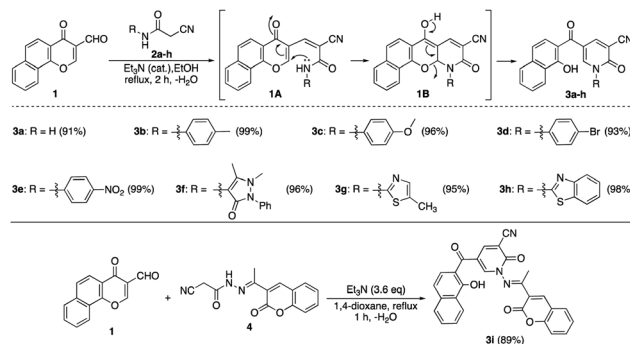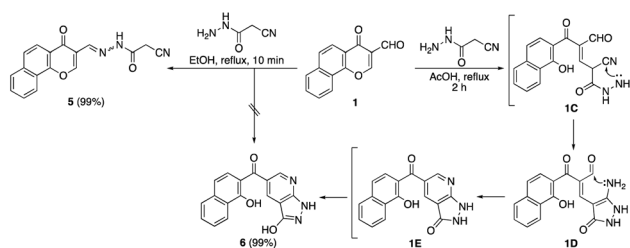

Scheme 1 Reaction of formylchromone 1 with cyanoacetanilides $2a–h$.

It was found that the reaction of formylchromone 1 with cyanoacetic acid hydrazide instead of cyanoacetanilide $2a$ by heating in ethanol afforded product 5 as a mixture of hydrazone and azo tautomers. In acetic acid, the reaction proceeded via γ-pyrone ring opening to give the novel naphthyl pyrazolopyridine 6 in 99% yield. Compound 6 gave a dark red color with $FeCl_3$ solution, indicating the presence of the free phenolic OH group. The proposed pathway included 1,4-conjugate addition to the α,β-unsaturated carbonyl moiety of formylchromone 1 followed by γ-pyrone ring opening to give intermediate $1C$. After that, hydrazido NH_2 attacked the nearby cyano function to afford aminopyrazolone intermediate $1D$ which transformed into intermediate $1E$ through the intramolecular condensation of its amino group with the pendant formyl group. Finally, intermediate $1E$ gave naphthyl pyrazolopyridine ketone 6 by keto to enol tautomerization (Scheme 2).

The scope of this tandem process was extended by the reaction of formylchromone 1 with 1,4-N,N- and 1,4-N,S-dinucleophiles as shown in Scheme 3. Initially, the reaction of precursor 1 with thiosemicarbazide afforded the corresponding naphthyl triazepine ketones 7 in excellent yields. Similarly, the reaction with o-aminothiophenol afforded naphthyl thiazepine ketone 8 in 98% yield. Formation of thiosemicarbazone or imine intermediates could be the first step in the formation of products 7 and 8 followed by spontaneous γ-pyrone ring opening via intramolecular cyclization by the aid of the second nucleophilic center whether NH_2 or SH.

The reaction of formylchromone 1 with hydrazine hydrate (1,2-N,N-dinucleophile) at room temperature proceeded via an unexpected tandem pathway to give novel chromenopyrazole 10

Fig. 2 Design of new naphthalene hybrid skeletons.

Scheme 2 Reaction of formylchromone 1 with cyanoacetic acid hydrazide.
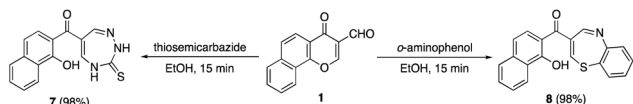
Scheme 3 Reaction of formylchromone **1** with thiosemicarbazide and *o*-aminothiophenol.

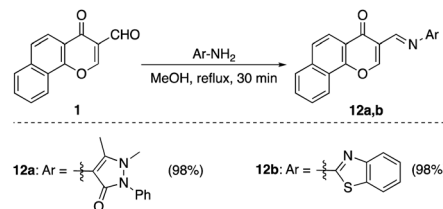**Scheme 5** Reaction of formylchromone **1** with 4-aminoantipyrine and 2-aminobenzothiazole.

instead of naphthyl pyrazolyl ketone **9**. Moreover, the presence of acetal functionality in compound **10** offers an excellent platform for further functionalization through the reaction with different nucleophiles (Scheme 4).[26]

By performing the reaction of formylchromone **1** with hydrazine in a ratio of 1 : 2 in boiling ethanol, hydrazineylidenomethylpyrazole **11** was obtained in excellent yield. The intermediacy of chromenopyrazole **10** in this transformation was confirmed by the conversion of **10** into **11** by the reaction with one equivalent hydrazine. Our proposed mechanistic pathway involved the formation of hydrazone intermediate **1F** which couldn't be converted into naphthyl pyrazolyl ketone **9** due to the addition of ethanol molecule to give intermediate **1G**. The absence of ethanol reversible elimination pathway suggested possible role of hydrogen bonding between NH and carbonyl oxygen to stabilize intermediate **1G**. While the formation of chromenopyrazole **10** could be accomplished by dehydration, its over-reaction with one equivalent hydrazine afforded pyrazole **11** *via* nucleophilic attack at acetal carbon followed by ring-opening.

Finally, the reaction with primary heterocyclic amines namely; 4-aminoantipyrine and 2-benzothiazolamine afforded the corresponding Schiff bases **12a,b** respectively in excellent yields. The reaction proceeded as a simple condensation without ring-opening of γ-pyrone, which was confirmed by a negative ferric chloride test to support the absence of a phenolic hydroxyl group (Scheme 5).

Biological evaluation

Prediction of biological activities and estimation of the pharmacokinetic parameters. The PASS online predictor was

used to predict the putative biological activity spectrum of the synthesized derivatives (ESI 2†).[2d,e] It compares structural descriptors for these derivatives with descriptors of biologically active compounds available in the database. This tool provides predictions correlating P_a (probability to be active) with P_i (probability to be inactive). Results for the activity prediction illustrated that the synthesized compounds may show a broad spectrum of biological activities *e.g.* anticancer, antimicrobial, antiviral, antiprotozoal, anti-inflammatory, *etc.* In this study, we focused on testing the anticancer, anti-inflammatory, and antituberculosis activities for the synthesized compounds. Also, pharmacokinetics and drug-likeness prediction for the derivatives were explored (ESI 1†).[2d,e]

The physicochemical parameters are molecular weight (MW), count of specific atom types (hydrogen donors, hydrogen acceptors, and rotatable bonds), and topological polar surface area (TPSA) that represents the surface associated with polar atoms. Compounds **3c**, **3e**, **3f**, **3i**, and **5** with four rotatable bonds suggested their better interaction ability. Moreover, compounds **3e** and **3i** showed six and seven hydrogen bond acceptors, respectively. Regarding lipophilicity, most of the synthesized compounds gave log *P* values below five indicating their good cell membrane permeability. Most of the synthesized compounds showed good water solubility suggesting their better delivery even upon using small doses.[27] Since the bioactivity score describes the positive medicinal impacts of putative drugs, all compounds were found to have a score of 0.55 suggesting higher biological activities in the clinical trial stage.[28]

Antitumor activity. The synthesized compounds were *in vitro* evaluated for their cytotoxic activities using MTT assay on two different human cancer cell lines (HepG-2 and MCF-7). The percentages of the viable cells and their IC$_{50}$ values were measured and assessed with those of the control, Doxorubicin (DOXO) (Fig. 3 and 4; Table 1). The results revealed that all compounds presented dose-dependent cytotoxicity activities against both cell varieties (Fig. 3 and 4). Regarding HepG-2 and compared to Doxorubicin, compounds **3c**, **3e**, and **3h** were more potent; compounds **3g** and **7b** displayed comparable cytotoxic activities; compounds **3d**, **3f**, and **3i** had slightly reduced activities; compounds **3a**, **3b**, **6**, **8**, **10**, **11**, and **12a** had moderate activities, however, compounds **5** and **12b** had weak activities (Fig. 3 and Table 1). In the case of MCF-7, compounds **3a–e**, **3i**, **6**, **8**, **10**, **11**, and **12b** were more potent; compounds **3f**, **3h**, **5**, **7b**, and **12a** displayed comparable cytotoxic activities; compound **3g** had slightly reduced activities compared to the positive control (Fig. 4 and Table 1).
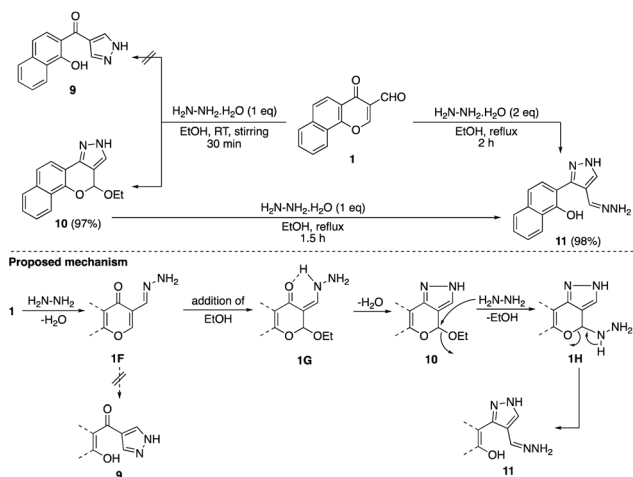
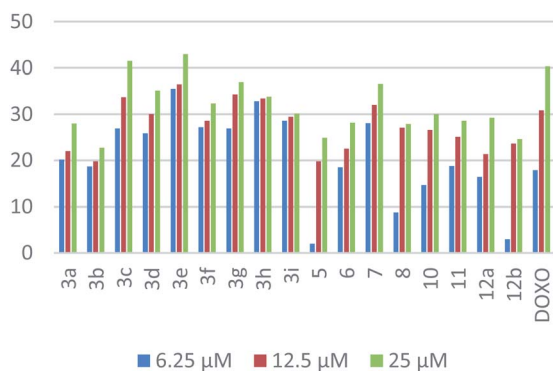**Scheme 4** Reaction of formylchromone **1** with hydrazine hydrate.

Fig. 3 Dose-dependent cytotoxic activities for the synthesized compounds on HepG-2.
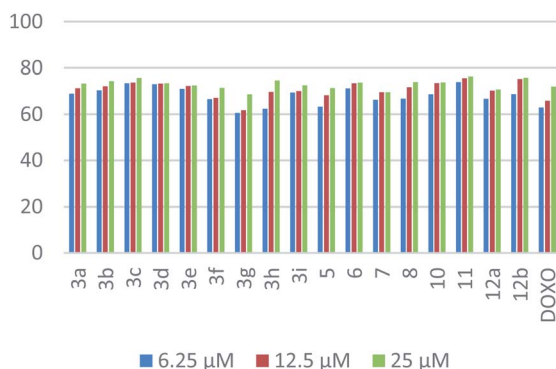

Fig. 4 Dose dependent cytotoxic activities for the synthesized compounds on MCF-7.

In the case of HepG-2, the superiority of naphthalene–nicotinonitrile hybrid as seen in the *p*-nitrophenyl derivative **3e** compared to other nicotinonitrile derivatives emphasized the significance of the nitro group. The antitumor activity decayed gradually by changing the nitrogen substituent as in the order of **3c** > **3h** > **3g** > **3d** > **3f** > **3i** > **3a** > **3b**. Moreover, macrocyclic segment of the naphthalene–azepine hybrid with three nitrogen atoms (1,2,4-triazepine; **7**) revealed enhanced activity compared to its closely related analog with nitrogen and sulfur atoms (1,4-thiazepine; **8**). Merging of naphthalene and pyrazole as in compound **11** appeared as a better hybrid than that of naphthalene and pyran (compound **12a**). The combination of the three motifs together in one ternary hybrid (compound **10**) produced an antitumor activity resembling naphthalene–pyrazole hybrid **11**. Finally, the activity of naphthalene–pyran hybrid degraded by changing the attached substituent from imine into hydrazone as seen in the order of **12a** > **12b** > **5**.

In the case of MCF-7, naphthalene–pyrazole hybrid (compound **11**) appeared as the most superior antitumor compound followed by the naphthalene–nicotinonitrile bearing *p*-methoxyphenyl substituent **3c**. The activity of naphthalene–nicotinonitrile hybrids decreased by changing the nitrogen substituents from *p*-substituted phenyl groups (**3c** > **3d** > **3b** > **3e**) into non-substituted parent (**3a**), and then coumarylimino (**3i**) followed by 5-membered heterocyclic substituents (**3h** > **3f** > **3g**). Regarding naphthalene–pyran hybrids, the activity was lessened in the view of the attached moiety as seen in the order of **12b** > **12a** > **5**. Finally, the hybrid with 1,4-thiazepine (**8**) appeared to be more active than the one with 1,2,4-triazepine (**7**).

In order to assess the selectivity of the synthesized compounds for human liver and breast cancer cell lines,

Table 1 Cytotoxic activities and molecular docking results of the synthesized compounds against 2I4I and 5GWK

	IC_{50} (µM) ± SD		PDB 2I4I		PDB 5GWK	
Comp.	HepG-2	MCF-7	Binding affinity (kcal mol^{-1})	Amino acid involved in hydrogen bonds	Binding affinity (kcal mol^{-1})	Amino acid involved in hydrogen bonds
3a	34.6 ± 3.3	9.6 ± 0.7	−7.4	ARG-531, ARG-534	−7.3	LYS-197
3b	36.8 ± 3.9	9.2 ± 0.6	−8.1	ARG-531, ARG-534	−7.8	LYS-197, GLU-194
3c	27.8 ± 2.4	8.5 ± 0.7	−8.3	ARG-531, ARG-534, ARG-202, LYS-208	−7.7	LYS-197
3d	30.1 ± 2.6	8.9 ± 0.7	−7.6	ARG-531, ARG-534	−7.6	LYS-197
3e	25.3 ± 2.1	9.3 ± 1.1	−8.8	ARG-531, ARG-534, ARG-202	−8.7	SER-361, MET363
3f	30.5 ± 3.1	10.5 ± 1.1	−8.8	ARG-531, ARG-534, ILE-507, HIS-527	−8.7	SER-198, ARG-402, ASP-258
3g	28.5 ± 2.9	12.1 ± 1.2	−8.2	SER-228, THR-204	−7.7	LYS-197, GLU-194
3h	28.1 ± 3.1	10.3 ± 1.2	−8.2	HIS-527	−8.6	ARG-402, GLU-194
3i	30.5 ± 2.9	9.7 ± 0.8	−9.2	HIS-527, ARG-534, GLY-504	−8.8	GLU-194, SER-361, SER-198, LEU-362
5	41.6 ± 3.5	10.7 ± 1.2	−7.7	HIS-527, ARG-202, ARG-531	−7.3	LEU-362
6	34.9 ± 2.8	9.1 ± 0.5	−7.2	—	−7.7	ARG-402, ASP-258, ASP-257
7	28.8 ± 2.5	10.5 ± 0.9	−6.8	ARG-531, ARG-534	−7.7	ARG-402, ASP-258, SER-400
8	36.5 ± 3.4	9.7 ± 1.1	−7.4	ARG-531, ARG-534	−7.8	—
10	34.5 ± 2.6	9.3 ± 0.5	−7.3	ARG-534, HIS-527	−6.8	SER-361
11	34.1 ± 3.1	8.2 ± 0.6	−6.2	ARG-531, ARG-534	−6.5	LYS-197, GLU-194
12a	35.5 ± 3.6	10.2 ± 1.2	−7.9	—	−8.1	PRO-191
12b	40.1 ± 3.9	8.9 ± 0.7	−7.7	—	−7.7	GLU-194
DOXO	28.5 ± 1.9	10.3 ± 0.8	−7.7	ARG-202, ARG-531, ARG-534, GLY-504, LYS-208	−7.9	GLU-194, SER-198

Autodock was used to predict the binding pose with active sites of two protein targets (2I4I and 5GWK) (Table 1). The anticancer Doxorubicin was also docked on the targets for comparison purposes. The lowest energy docking mode and the best conformation pose, having the best affinity for a molecule out of ten docking modes obtained by Lamarckian Genetic Algorithm (LGA cluster analysis with respective predicted IC_{50}), were selected from each docking simulation. The polar interactions with the two protein targets were illustrated (Table 1). However, the binding energies of compounds **3e**, **3c**, and **3h** were in good agreement with the experimental data, docking scores for compounds **3f** and **3i** were not. For examples, compound **3c** showed identical binding modes that involved polar interactions with ARG-531, ARG-534, ARG-202, and LYS-208 residues in 2I4I (Fig. 5A); compound **3e** were hydrogen-bonded with ARG-531, ARG-534, and ARG-20 residues in 2I4I (Fig. 5B); while compound **3h** revealed hydrogen bonding with HIS-523 residue in 2I4I (Fig. 5C).

Similarly, the hydroxyl group of naphthalene in compound **3c** were included in polar interactions with LYS-197 in 5GWK (Fig. 5D); compound **3e** showed polar interactions with SER-361 and MET-363 in 5GWK (Fig. 5E); while compound **3h** had polar interactions with ARG-402, and GLU-194 in 5GWK (Fig. 5F). Besides, naphthalene played a major role in the binding affinities of different compounds against the two cancer cell lines. For example, compound **3c** was stabilized through π-interactions between the naphthalene with SER-228, GLN-225, GLY-406, and THR-411 in 2I4I; and ALA-350, GLY-347, LEU-362, SER-198, and GLU-194 in 5GWK (ESI 1†).

Anti-inflammatory activity. Non-steroidal anti-inflammatory drugs (NSAIDs) inhibit cyclooxygenases (COX) which promote the generation of prostaglandins from arachidonic acid. The therapeutic efficiency of NSAIDs was measured based upon the selectivity towards COX-2 over COX-1 which produced undesired side effects such as renal and gastrointestinal toxicity upon inhibition. As a result, the more COX-2 selective inhibitor, the more efficient NSAID.[29] Screening of the synthesized compounds over COX-1 and COX-2 enzymes revealed that many compounds (**3c** > **3h** > **8** > **10** > **3d** > **12b**) were more active and selective than the reference anti-inflammatory Celecoxib (CEL)
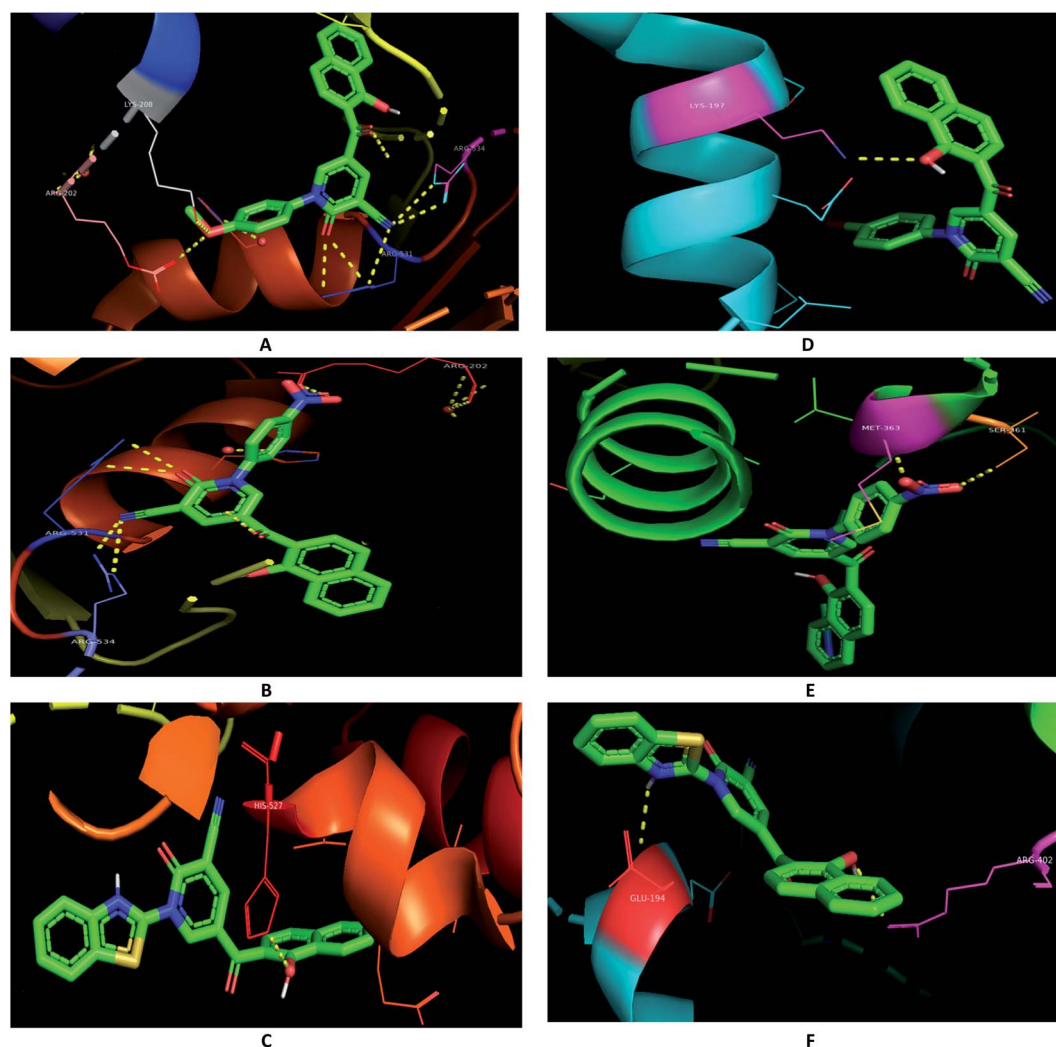

Fig. 5 Binding modes (A) **3c** and 2I4I; (B) **3e** and 2I4I; (C) **3h** and 2I4I; (D) **3c** and 5GWK; (E) **3e** and 5GWK; (F) **3h** and 5GWK.

(Table 2). While compounds **7**, **3e**, and **3i** appeared to be promising candidates, other derivatives showed decreased selectivity.

Based upon judicious analysis of the structure–activity relationships (SARs), the utility to cap the NH group in the case of hybrid **3** to suppress the tautomerization of lactam into lactim was highlighted by the potent activity of naphthalene–nicotinonitrile **3c** compared to **3a**. The anti-inflammatory activities of other naphthalene–nicotinonitrile derivatives were decreased in the order of **3h** > **3d** > **3e** > **3i** > **3b** > **3g** > **3f** > **3a**. However, the naphthalene–thiazepine hybrid appeared to be more selective than Celecoxib, naphthalene–triazepine revealed inferior selectivity. The formation of a ternary hybrid between naphthalene, pyran, and pyrazole (compound **10**) or at least a binary hybrid between naphthalene and pyran (**12b**) was necessary to achieve high selectivity compared to the binary hybrid between naphthalene and pyrazole (**11**). Compound **12b** as an example of naphthalene–pyran hybrid showed the importance of benzothiazole moiety compared to other analogous compounds **12a** and **5**. Finally, the combination of naphthalene and pyrazolopyridine moieties was found very deleterious as seen in the least selective anti-inflammatory derivative **6**.

The molecular docking of the synthesized compounds in addition to the anti-inflammatory Celecoxib with the drug target COX-2 domains supported the experimental screening in the view of binding energies (Table 2). The binding energies on COX-2 were found in the range of 7.7–12.2 kcal mol^{-1}. As seen in Table 2, compounds **3c** and **3h** were noted to have the best estimated binding energies for COX-2. However, several amino acid residues were involved in the binding mode, only one polar interaction was shown with ARG-345 residue in 4PH9 (Fig. 6). Besides, the naphthalene skeleton increased the binding
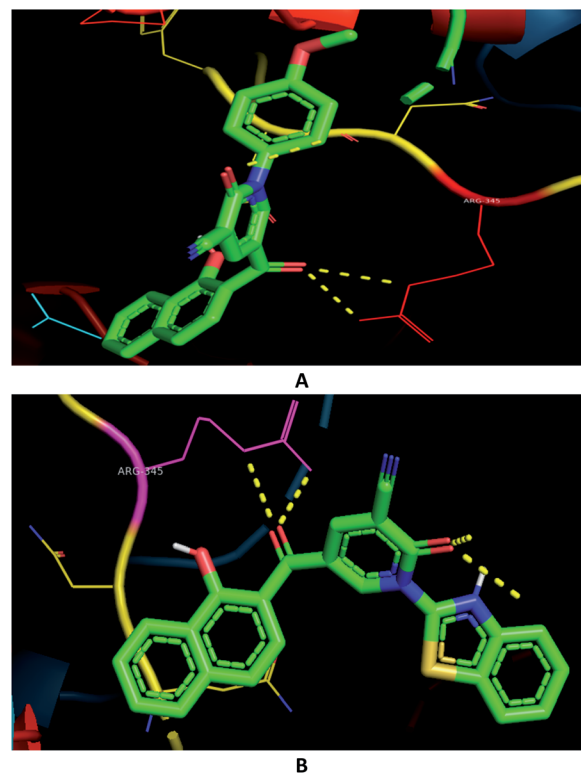

Fig. 6 Binding modes (A) **3c** and COX-2 (PDB 4PH9); (B) **3h** and COX-2 (PDB 4PH9).

affinities against COX-2. For example, compound **3c** was stabilized through π-interactions between the naphthalene with PRO-96, GLN-343, ASN-344, ASP-198, SER-112, and GLY-194 in 4PH9 (ESI†).

Table 2 Anti-inflammatory activities and molecular docking results of the synthesized compounds against COX-1 and COX-2

Comp.	IC$_{50}$^{a} (µg mL^{-1})		Selectivity index (SI)^{b}	COX-2 (PDB 4PH9)	
	COX-1	COX-2		Binding affinity (kcal mol^{-1})	Amino acid involved in hydrogen bonds
3a	124.6	8.1	15.4	−8.8	ARG-345
3b	176.4	2.3	76.7	−10.6	GLN-343, ARG-345
3c	312.9	0.21	1490	−10.2	ARG-345
3d	632.4	0.65	972.9	−9.7	ARG-345
3e	116.4	0.69	168.7	−11	GLN-343, ASN-506, ARG-345
3f	346.9	7.8	44.5	−10.7	ARG-345
3g	1000	18.6	53.8	−10.5	GLN-343, ARG-345
3h	289.8	0.21	1380	−10.8	ARG-345
3i	712.5	6.4	111.3	−12.2	GLN-343, ARG-345
5	632.4	7.5	84.3	−9.5	ASN506, ASN-344
6	325.6	9.3	35.0	−9.5	ARG-345
7	217.8	0.37	588.6	−9.3	—
8	284.5	0.25	1138	−9.3	ARG-345
10	267.1	0.27	989.3	−7.7	GLN-343
11	1000	12.1	82.6	−7.7	GLN-343, ARG-345
12a	500	10.1	49.5	−10.5	—
12b	476.2	0.49	971.8	−9	—
CEL	248.9	0.26	957.3	−9	—

^{a} It is the compound concentration required to produce 50% inhibition of COX-1 or COX-2. ^{b} Selectivity index = (COX-1 IC$_{50}$/COX-2 IC$_{50}$).

Table 3 Antituberculosis activities and molecular docking results of the synthesized compounds against InhA enzyme

| Comp. | MIC (μg mL^{-1}) | PDB 4DRE | | |
		Binding affinity (kcal mol^{-1})	Amino acid involved in hydrogen bonds	
3a	15.63	−8.1	ILE-257	
3b	3.9	−9.1	ILE-257	
3c	0.48	−9.0	ARG-153, ASP-256	
3d	0.98	−9.1	ASP-256	
3e	1.95	−9.6	ARG-153, ASP-256,	
3f	1.95	−10.5	ARG-173, GLU-169, TYR-259	
3g	3.9	−8.9	ASP-256	
3h	1.95	−9.3	ARG-153, ARG-173	
3i	0.98	−10.7	ARG-153, ARG-173	
5	3.9	−8.3	GLU-169, ARG-173, SER-166	
6	1.95	−8.5	HIS-265, ARG-153	
7	1.95	−7.6	ASP-256, GLU-169	
8	7.81	−8.1	TYR-259	
10	7.81	−7.3	ASP-256	
11	31.25	−7.6	ARG-173, SER-152, SER-166	
12a	62.5	−9.4	ARG-153	
12b	15.63	−9.1	ARG-153	
IN	0.24	−4.8	GLU-169, SER-166, SER-152	

Antituberculosis activity. Testing of the synthesized compounds against *Mycobacterium tuberculosis* (RCMB 010126) strain was performed *in vitro*. The antituberculosis drug Isoniazid (IN) was used as a reference, and the results were presented as minimum inhibition concentration (MIC) as shown in Table 3. Among the compounds we tested, **3c, 3d**, and **3i** were found to be the most promising with MIC less than 1 μg mL^{-1}. Additionally, compounds **3e, 3f, 3h, 6**, and **7** gave MIC values less than 2 μg mL^{-1}.

The excellence of the naphthalene–nicotinonitrile hybrid scaffold was assured by the higher activity of compounds **3c, 3d**, and **3i**. Moreover, the poor antituberculosis activity of compound **3a**, highlighted the need to cap the NH group to retain high antituberculosis activity levels. Protection with *p*-methoxyphenyl group appeared to be the optimum compared to other protecting groups in derivatives **3d, 3i, 3e, 3f, 3h, 3b**, and **3g**. Guided by the equal MICs of compounds **3e–h, 6**, and **7**, pyrazolopyridine or triazepine moieties produced the same activity observed in substituted nicotinonitrile derivatives **3e–h**.

Fig. 7 Binding of **3c** with *M. tuberculosis* InhA (PDB 4DRE).

Moreover, the activity of compound **7** was significantly decayed by replacement of triazepine with thiazepine moiety as seen in compound **8**. The combination of naphthalene and pyran moieties as in compound **5** appeared to be superior to compound **10** with the naphthalene–pyranopyrazole and compound **11** with the naphthalene–pyrazole skeleton.

Based on molecular docking analysis, compound **3c** was seen to have two polar interactions with ARG-153, ASP-256 residues (Fig. 7), and π-interactions between the naphthalene skeleton with ILE-257, HIS-265, and SER-152 in 4DRE (ESI†). In addition, compounds **3d, 3e, 3f, 3h**, and **3i** appeared to be good candidates.

Conclusion

Novel hybrid naphthalene compounds with different heterocyclic scaffolds have been synthesized *via* tandem reactions of 3-formylchromone with different nucleophilic reagents such as cyanoacetanilides, cyanoacetic acid hydrazide and its hydrazone, thiosemicarbazide, *o*-aminothiophenol, hydrazine, and heterocyclic °1-amines. Different predicted biological activities have been disclosed based upon analysis using PASS online software. Experimentally, different compounds revealed potent antitumor, anti-inflammatory and antituberculosis activities. Compared to the antitumor Doxorubicin, compounds **3c, 3e**, and **3h** were more cytotoxic in the case of HepG-2, and compounds **3a–e, 3i, 6, 8, 10, 11**, and **12b** were more cytotoxic against MCF-7. While compounds **3c, 3h, 8, 10, 3d**, and **12b** appeared as potent COX-2 selective anti-inflammatory agents, compounds **3c, 3d**, and **3i** revealed promising antituberculosis activity with MIC less than 1 μg mL^{-1}. A strong agreement between PASS predictions, pharmacokinetic properties, experimental biological evaluations, and docking results were noticed. Molecular docking showed strong polar and hydrophobic interactions between the novel naphthalene-heterocycle hybrids and multifunctional drug targets. Further extensive studies including *in vivo* studies and approaching more optimized hybrid naphthalene skeletons in addition to the unveiling of the mechanism of action (MOA) of potent compounds are currently underway.

Experimental section

General

All melting points in this study were measured by using the Gallenkamp electrical melting point device and reported using the celsius scale. The infrared absorptions of new compounds as potassium bromide pellets were measured on a Mattson 5000 FT-IR spectrophotometer (Faculty of Pharmacy, Mansoura University, Egypt) or Thermo Fisher Nicolete iS 10, USA (Faculty of Science, Mansoura University, Egypt). The ^{1}H- and ^{13}C-NMR spectra were measured on Bruker Avance III 400 MHz (Faculty of Pharmacy, Mansoura University or Faculty of Pharmacy, Beni Suef University, Egypt), and/or JEOL ECA II 500 MHz (Faculty of Science, Mansoura University, Egypt) using tetramethylsilane as an internal reference. The multiplicities of NMR signals were reported as: s = singlet, d = doublet, dd = doublet of doublets, t
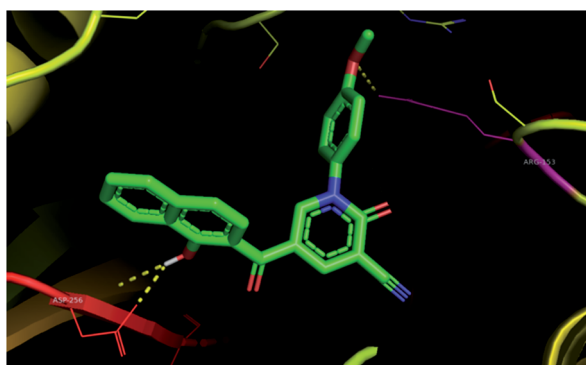
= triplet, q = quartet and m = multiplet. ^{13}C NMR spectra were measured on JEOL ECA II 125 MHz (Faculty of Science, Mansoura University, Egypt). The EI-Mass analyses were performed on Thermo Fisher scientific DSQ II GC/MS with Kratos MS-70 ev (Faculty of Pharmacy, Al-Azhar University, Egypt). C, H, and N analyses were carried at the microanalytical unit, Cairo University, Egypt. For high-resolution mass spectrometry (HRMS) was performed using Thermo Fisher Scientific Q Exactive Hybrid Quadrupole-Orbitrap Mass Spectrometer (College of Pharmacy, Chung-Ang University, South Korea) and m/z ratios were reported as values in atomic mass units.

Synthesis

General procedure for the synthesis of heteroaryl napthyl ketones 3a–h. An equimolecular mixture of formylchromone 1 (1 mmol, 224 mg) and acetanilides 2a–h (1 mmol) in absolute ethanol (30 mL) in the presence of with a catalytic amount of Et$_3$N was refluxed. After that, the formed precipitate was filtered off, washed with hot ethanol, and dried to give corresponding heteroaryl naphthyl ketones 3a–h.

5-(1-Hydroxy-2-naphthoyl)-2-oxo-nicotinonitrile (3a).
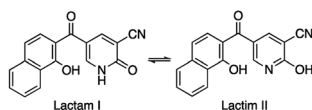
It is a tautomeric mixture in 4 : 1 ratio. Yield (263 mg, 91%); canary yellow crystals; m.p. = 346–347 °C; IR (KBr, ν/cm^{-1}) = 3375, 3367, 3175 (2× OH, NH), 2231 (CN), 1706 (CO$_{Ketone}$), 1630 (CO$_{Pyridone}$); ^{1}H-NMR (500 MHz, DMSO-d$_6$) δ (ppm): 7.48–7.46 (m, 1H, Ar–H, I and II), 7.62–7.57 (m, 2H, Ar–H, I and II), 7.71–7.68 (m, 1H, Ar–H, I and II), 7.77 (d, 1H, Ar–H, J = 4.50 Hz, I or II), 7.94 (d, 1H, Ar–H, J = 8.30 Hz, I or II), 8.15 (d, 1H, Ar–H (pyridyl), J = 2.70 Hz, I or II), 8.21 (d, 1H, Ar–H (pyridyl), J = 2.00 Hz, I or II), 8.35 (d, 1H, Ar–H, J = 8.30 Hz, I or II), 8.49 (d, 1H, Ar–H (pyridyl), J = 2.00 Hz, I or II), 8.67 (d, 1H, Ar–H (pyridyl), J = 2.70 Hz, I or II), 8.80 (d, 1H, Ar–H, J = 4.50 Hz, I or II), 12.26 (brs, 1H, OH or NH, exchangeable with D$_2$O), 13.01 (brs, 1H, OH or NH, exchangeable with D$_2$O); HRMS (ESI): m/z calcd for C$_{17}$H$_{10}$N$_2$NaO$_3$ [(M + Na)$^+$] 313.0584, found 313.0576; anal. calcd for C$_{17}$H$_{10}$N$_2$O$_3$ (290.07): C, 70.34; H, 3.47; N, 9.65%. Found: C, 70.54; H, 3.49; N, 9.61%.

5-(1-Hydroxy-2-naphthoyl)-2-oxo-1-(p-tolyl)nicotinonitrile (3b). Yield (375 mg, 99%); yellow crystals; m.p. = 288–289 °C; IR (KBr, ν/cm^{-1}) = 3650–3340 (br. OH), 2231 (CN), 1681 (CO$_{Ketone}$), 1622 (CO$_{Pyridone}$); ^{1}H NMR (400 MHz, CDCl$_3$) δ (ppm): 2.46 (s, 3H, CH$_3$), 7.32 (d, 1H, naphthyl–H, J = 10.00 Hz), 7.41–7.34 (m, 4H, Phenyl–H), 7.49 (d, 1H, naphthyl–H, J = 10.43 Hz), 7.58 (dd, 1H, naphthyl–H, J = 9.20, 10.00 Hz), 7.72 (dd, 1H, naphthyl–H, J = 9.00, 10.00 Hz), 7.82 (d, 1H, naphthyl–H, J = 10.00 Hz), 8.28 (d, 1H, pyridone–H, J = 3.00 Hz), 8.35 (d, 1H, pyridone–H, J = 3.00 Hz), 8.51 (d, 1H, naphthyl–H, J = 10.43 Hz), 13.26 (s, 1H, OH, exchangeable with D$_2$O); ^{13}C NMR (150 MHz, CDCl$_3$) δ (ppm): 192.9, 163.8, 158.6, 147.1, 147.0, 140.4, 137.4, 136.4, 131.0, 130.4, 127.6, 126.6, 125.7, 125.3, 124.8, 124.6, 119.0, 117.0, 114.6, 111.4, 105.9, 21.2; EI-MS m/z (%): 76.24 (48.07%),

78.50 (63.29%), 90.13 (50.02%), 113.43 (63.00%), 114.12 (89.99%), 168.98 (89.13%), 380.28 (100.00), 382.35 (38.66%), 383.77 (2.68%); HRMS (ESI): m/z calcd for C$_{24}$H$_{16}$N$_2$NaO$_3$ [(M + Na)$^+$] 403.1053, found 403.1045; anal. calcd for C$_{24}$H$_{16}$N$_2$O$_3$ (380.12): C, 75.78; H, 4.24; N, 7.36%. Found: C, 75.81; H, 4.15; N, 7.39%.

5-(1-Hydroxy-2-naphthoyl)-1-(4-methoxyphenyl)-2-oxo-nicotinonitrile (3c). Yield (382 mg, 96%); pale orange crystals; m.p. = 262–263 °C; IR (KBr, ν/cm^{-1}) = 3330 (OH), 2228 (CN), 1678 (CO$_{Ketone}$), 1634 (CO$_{Pyridone}$); ^{1}H-NMR (400 MHz, CDCl$_3$) δ (ppm): 3.82 (s, 3H, OCH$_3$), 7.09 (d, 2H, phenyl–H, J = 8.79 Hz), 7.49 (d, 2H, phenyl–H, J = 8.79), 7.52–7.63 (m, 2H, naphthyl–H), 7.88–7.71 (m, 2H, naphthyl–H), 7.95 (d, 1H, naphthyl–H, J = 8.15 Hz), 8.38 (d, 1H, naphthyl–H, J = 8.15 Hz), 8.44 (d, 1H, pyridone–H, J = 2.46 Hz), 8.62 (d, 1H, pyridone–H, J = 2.46 Hz), 11.67 (s, 1H, OH, exchangeable with D$_2$O); EI-MS m/z (%): 159.30 (100.00), 161.03 (58.27%), 172.30 (73.20%), 191.98 (72.16%), 207.55 (58.96%), 296.67 (64.83%), 396.25 (22.10%); HRMS (ESI): m/z calcd for C$_{24}$H$_{16}$N$_2$NaO$_4$ [(M + Na)$^+$] 419.1002, found 419.1002; anal. calcd for C$_{24}$H$_{16}$N$_2$O$_4$ (396.11): C, 72.72; H, 4.07; N, 7.07%. Found: C, 72.80; H, 4.01; N, 7.04%.

1-(4-Bromophenyl)-5-(1-hydroxy-2-naphthoyl)-2-oxo-nicotinonitrile (3d). Yield (413 mg, 93%); green crystals; m.p. = 330–331 °C; IR (KBr, ν/cm^{-1}) = 3304 (OH), 2225 (CN), 1667 (CO$_{Ketone}$), 1642 (CO$_{Pyridone}$); ^{1}H-NMR (400 MHz, CDCl$_3$) δ (ppm): 7.77–7.46 (m, 4H, phenyl–H), 7.99–7.79 (m, 2H, naphthyl–H), 8.15 (d, 1H, naphthyl–H, J = 9.20 Hz), 7.94 (d, 1H, naphthyl–H, J = 9.20 Hz), 8.05 (d, 1H, naphthyl–H, J = 8.18 Hz), 8.53 (d, 1H, naphthyl–H, J = 8.15 Hz), 8.75 (s, 1H, pyridone–H), 9.34 (s, 1H, pyridone–H), 10.34 (s, 1H, OH); EI-MS m/z (%): 165.36 (63.52%), 211.13 (74.29%), 253.69 (61.72%), 321.12 (97.78%), 340.00 (75.22%), 378.38 (100.00), 444.17 (29.06%); HRMS (ESI): m/z calcd for C$_{23}$H$_{12}$BrN$_2$O$_3$ [(M − H)$^-$] 364.0842, found 364.0854; anal. calcd for C$_{23}$H$_{13}$BrN$_2$O$_3$ (444.01): C, 62.04; H, 2.94; Br, 17.94; N, 6.29%. Found: C, 62.11; H, 2.99; Br, 17.85; N, 6.14%.

5-(1-Hydroxy-2-naphthoyl)-1-(4-nitrophenyl)-2-oxo-nicotinonitrile (3e). Yield (405 mg, 99%); green crystals; m.p. = 320–322 °C; IR (KBr, ν/cm^{-1}) = 3650–3290 (br. OH), 2224 (CN), 1665 (CO$_{Ketone}$), 1646 (CO$_{Pyridone}$); ^{1}H-NMR (400 MHz, CDCl$_3$) δ (ppm): 7.96–7.69 (m, 4H, phenyl–H), 8.15–8.01 (m, 2H, naphthyl–H), 8.29–8.17 (m, 2H, naphthyl–H), 8.58–8.35 (m, 2H, naphthyl–H), 8.67 (s, 1H, pyridone–H), 8.78 (s, 1H, pyridone–H), 10.82 (s, 1H, OH); EI-MS m/z (%): 77.29 (71.91%), 105.80 (58.71%), 128.99 (62.83%), 134.41 (86.53%), 328.22 (100.00), 403.45 (80.36%), 411.40 (50.29%); HRMS (ESI): m/z calcd for C$_{23}$H$_{13}$N$_3$NaO$_5$ [(M + Na)$^+$] 434.0747, found 434.0730; anal. calcd for C$_{23}$H$_{13}$N$_3$O$_5$ (411.09): C, 67.15; H, 3.19; N, 10.21%. Found: C, 67.11; H, 3.24; N, 10.25%.

1-(1,5-Dimethyl-3-oxo-2-phenyl-2,3-dihydro-1H-pyrazol-4-yl)-5-(1-hydroxy-2-naphthoyl)-2-oxo-nicotinonitrile (3f). Yield (456 mg, 96%); orange crystals; m.p. = 354–355 °C; IR (KBr, ν/cm^{-1}) = 3554–3340 (OH), 2223 (CN), 1680 (CO$_{Ketone}$), 1624 (CO$_{Pyridone}$); ^{1}H-NMR (400 MHz, DMSO-d$_6$): δ (ppm): 2.28 (s, 3H, CH$_3$), 3.26 (s, 3H, NCH$_3$), 7.44–7.42 (m, 3H, phenyl–H), 7.49 (d, 1H, Ar–H, J = 8.76 Hz), 7.56 (dd, 2H, Ar–H, J = 7.71, 7.78 Hz), 7.63 (dd, 1H, Ar–H, J = 7.13, 7.71 Hz), 7.67 (d, 1H, Ar–H, J = 8.76 Hz), 7.73 (dd, 1H, Ar–H, J = 7.13, 7.78 Hz), 7.96 (d, 1H, Ar–H, J = 8.08 Hz), 8.38 (d, 1H, Ar–H, J = 8.08 Hz), 8.50 (d, 1H, pyridone–H, J = 2.46 Hz), 8.61 (d,

1H, pyridone–H, J = 2.46 Hz), 12.39 (s, 1H, OH, exchangeable with D$_2$O); EI-MS m/z (%): 313.64 (91.61%), 330.71 (83.93%), 344.56 (100.00), 394.29 (53.22%), 415.22 (78.71%), 438.42 (69.80%), 476.87 (38.31%), 477.65 (5.28%); HRMS (ESI): m/z calcd for C$_{28}$H$_{20}$N$_4$NaO$_4$ [(M + Na)$^+$] 499.1377, found 499.1371; anal. calcd for C$_{28}$H$_{20}$N$_4$O$_4$ (476.15): C, 62.04; H, 2.94; Br, 17.94; N, 6.29%. Found: C, 62.11; H, 2.99; Br, 17.85; N, 6.14%.

5-(1-Hydroxy-2-naphthoyl)-1-(5-methylthiazol-2-yl)-2-oxo-nicotinonitrile (3g). Yield (366 mg, 95%); yellow crystals; m.p. = 300–301 °C; IR (KBr, ν/cm^{-1}) = 3520–3550 (OH), 2233 (CN), 1673 (CO$_{\text{Ketone}}$), 1622 (CO$_{\text{Pyridone}}$); ^{1}H-NMR (400 MHz, DMSO-d_6): δ (ppm): 2.49 (s, 3H, CH$_3$), 7.53 (d, 1H, H-4, J = 8.39 Hz), 7.16 (d, 1H, Ar–H, J = 1.14 Hz), 7.65 (dd, 1H, Ar–H, J = 7.23, 7.64 Hz), 7.71 (d, 1H, Ar–H, J = 8.39 Hz), 7.75 (dd, 1H, Ar–H, J = 7.23, 8.02 Hz), 7.98 (d, 1H, Ar–H, J = 8.02 Hz), 8.37 (d, 1H, Ar–H, J = 7.64 Hz), 8.68 (brs, 1H, Ar–H), 9.28 (brs, 1H, Ar–H), 12.26 (s, 1H, OH, exchangeable with D$_2$O); EI-MS m/z (%): 89.37 (50.27%), 98.25 (100.00), 208.68 (51.43%), 251.29 (59.99%), 271.44 (94.44%), 287.62 (44.27%), 387.13 (30.53%); HRMS (ESI): m/z calcd for C$_{21}$H$_{13}$N$_3$NaO$_3$S [(M + Na)$^+$] 410.0570, found 410.0561; anal. calcd for C$_{21}$H$_{13}$N$_3$O$_3$S (387.07): C, 65.11; H, 3.38; N, 10.85, S, 8.28%. Found: C, 65.08; H, 3.25; N, 10.91, S, 8.31%.

1-(Benzo[d]thiazol-2-yl)-5-(1–Hydroxy-2-naphthoyl)-2-oxo-nicotinonitrile (3h). Yield (415 mg, 98%); yellow crystals; m.p. = 344–346 °C; IR (KBr, ν/cm^{-1}) = 3560–3390 (OH), 2237 (CN), 1675 (CO$_{\text{Ketone}}$), 1626 (CO$_{\text{Pyridone}}$); ^{1}H-NMR (400 MHz, CDCl$_3$) δ (ppm): 7.59–7.54 (m, 4H, phenyl–H), 7.63 (d, 2H, naphthyl–H, J = 8.40 Hz), 7.99 (d, 2H, naphthyl–H, J = 8.00 Hz), 8.24 (d, 1H, naphthyl–H, J = 7.60 Hz), 8.42 (d, 1H, naphthyl–H, J = 7.60 Hz), 8.80 (s, 1H, pyridone–H), 8.53 (s, 1H, pyridone–H), 12.41 (s, 1H, OH, exchangeable with D$_2$O); EI-MS m/z (%): 308.04 (100.00), 350.68 (64.94%), 351.92 (69.73%), 352.59 (52.89%), 356.63 (64.03%), 383.91 (51.51%), 423.59 (19.68%), 425.82 (33.67%); HRMS (ESI): m/z calcd for C$_{24}$H$_{13}$N$_3$NaO$_3$S [(M + Na)$^+$] 446.0570, found 446.0560; anal. calcd for C$_{24}$H$_{13}$N$_3$O$_3$S (423.07): C, 68.08; H, 3.09; N, 9.92; S, 7.57%. Found: C, 68.11; H, 3.01; N, 9.99; S, 7.61%.

Synthesis of 5-(1-hydroxy-2-naphthoyl)-2-oxo-1-((1-(2-oxo-2H-chromen-3-yl)ethylidene)amino)nicotinonitrile (3i). A solution of hydrazide **4** (1 mmol, 269 mg) and Et$_3$N (3.6 eq., 3.6 mmol, 0.5 mL) in dry dioxane (5 mL) was added to a solution of formylchromone **1** (1 mmol, 224 mg) in hot dioxane (10 mL). After that, the reaction mixture was heated over a water bath for 1 h. After complete consumption of formylchromone **1**, the reaction mixture was poured into water/ice mixture to give a precipitate which was filtered off, dried, and recrystallized from EtOH to give pure product **10**. Yield (422 mg, 89%); yellow crystals; m.p. = 306–307 °C; IR (KBr, ν/cm^{-1}) = 3568–3310 (OH), 2227 (CN), 1728 (CO$_{\text{Coumarin}}$), 1670 (CO$_{\text{Ketone}}$), 1610 (CO$_{\text{Pyridone}}$); ^{1}H-NMR (400 MHz, CDCl$_3$): δ (ppm): 2.29 (s, 3H, CH$_3$), 7.44–7.37 (m, 1H, Ar–H), 7.63–7.52 (m, 2H, Ar–H), 7.75–7.64 (m, 2H, Ar–H), 7.77 (d, 1H, Ar–H, J = 8.03 Hz), 7.73 (d, 1H, Ar–H, J = 8.72 Hz), 7.93 (d, 1H, Ar–H, J = 7.86 Hz), 7.97 (d, 1H, Ar–H, J = 8.03 Hz), 8.38 (d, 1H, Ar–H, J = 8.36 Hz), 8.58 (brs, 1H, pyridone–H), 8.62 (s, 1H, coumarin–H), 8.66 (brs, 1H, pyridone–H), 12.15 (s, 1H, OH, exchangeable with D$_2$O); EI-MS m/z (%): 40.18 (100.00), 44.00 (27.41%), 327.24 (38.38%), 355.24 (43.70%), 356.29 (16.17%), 37.31 (4.99%), 474.76 (1.25%); HRMS (ESI): m/z calcd

for C$_{28}$H$_{17}$N$_3$NaO$_5$ [(M + Na)$^+$] 498.1060, found 498.1050; anal. calcd for C$_{28}$H$_{17}$N$_3$O$_5$ (475.12): C, 70.73; H, 3.60; N, 8.84%. Found: C, 70.69; H, 3.57; N, 8.96%.

Synthesis of 2-cyano-N'-((4-oxo-4H-benzo[h]chromen-3-yl)methylene)acetohydrazide (5). To a hot solution of formylchromone **1** (1 mmol, 224 mg) in absolute ethanol (15 mL), cyanoacetic acid hydrazide (1 mmol, 99 mg) in absolute ethanol (10 mL) was added with continuous stirring, and then the reaction mixture was refluxed for 10 min. The buff crystals, obtained during heating, were filtered off and crystallized from DMF/EtOH mixture to give compound **5** as a 3 : 1 mixture. Yield (301 mg, 98.69%); buff crystals; m.p. = 356–357 °C; IR (KBr, ν/cm^{-1}) = 3206 (NH), 2262 (CN), 1690 (CO$_{\text{Chromone}}$), 1639 (CO$_{\text{Hydrazide}}$), 1624 (C=N); ^{1}H NMR (400 MHz, DMSO-d_6): δ (ppm) = 4.27 (s, 2H, CH$_2$, E or Z), 3.88 (s, 2H, CH$_2$, E or Z), 7.83–7.82 (m, 2H, Ar–H, E and Z), 8.04–8.00 (m, 2H, Ar–H, E and Z), 8.13 (d, 1H, Ar–H, J = 7.68 Hz, E and Z), 8.19 (d, 1H, H-10, J = 7.68 Hz, E and Z), 8.48 (s, 1H, pyrone–H, E or Z), 8.32 (s, 1H, pyrone–H, E or Z), 8.95 (s, 1H, C̲H̲aN, E or Z), 9.06 (s, 1H, CH̲aN, E or Z), 11.89 (s, 1H, NH, exchangeable with D$_2$O, E or Z), 11.92 (s, 1H, NH, exchangeable with D$_2$O, E or Z); ^{13}C NMR (150 MHz, DMSO-d_6) δ (ppm): 174.5, 164.9, 153.9, 153.1, 136.6, 135.4, 129.9, 128.3, 128.0, 126.0, 123.2, 121.8, 120.0, 119.7, 119.4, 116.1, 24.2; EI-MS m/z (%): 40.19 (100.00), 44.09 (21.59%), 69.19 (1.58%), 113.89 (1.57%), 299.48 (1.42%), 305.20 (3.90%), 306.12 (2.18%); HRMS (ESI): m/z calcd for C$_{17}$H$_{11}$N$_3$NaO$_3$ [(M + Na)$^+$] 328.0693, found 328.0682; anal. calcd for C$_{17}$H$_{11}$N$_3$O$_3$ (305.08): C, 66.88; H, 3.63; N, 13.76%. Found: C, 66.94; H, 3.62; N, 13.85%.

Synthesis of 5-(1-hydroxy-2-naphthoyl)-3-hydroxy-1H-pyrazolo [3,4-b]pyridine (6). A mixture of formylchromone **1** (1 mmol, 224 mg) and cyanoacetic acid hydrazide (1 mmol, 99 mg) in acetic acid (10 mL) was refluxed for 2 h. The obtained crystals during heating were filtered and crystallized from acetic acid to give compound **6**. Yield (302 mg, 99%); pale orange crystals; m.p. = 352–354 °C; IR (KBr, ν/cm^{-1}) = 3580–3415 (OH), 3117 (NH), 1630 (CO$_{\text{Ketone}}$), 1603 (C=N); ^{1}H NMR (500 MHz, DMSO-d_6) δ (ppm): 7.48 (d, 1H, naphthyl–H, J = 8.65 Hz), 7.60 (d, 1H, naphthyl–H, J = 8.65 Hz), 7.65–7.63 (m, 1H, naphthyl–H), 7.75–7.73 (m, 1H, naphthyl–H), 7.96 (d, 1H, naphthyl–H, J = 8.15 Hz), 8.39 (d, 1H, naphthyl–H, J = 8.30 Hz), 8.49 (d, 1H, pyridine, J = 1.95 Hz), 8.82 (d, 1H, pyridine, J = 1.95 Hz), 11.30 (brs, 1H, OH or NH, exchangeable with D$_2$O), 12.75 (brs, 1H, OH or NH, exchangeable with D$_2$O), 12.88 (s, 1H, NH or OH, exchangeable with D$_2$O); ^{13}C NMR (150 MHz, DMSO-d_6) δ (ppm): 197.7, 159.6, 150.6, 136.5, 132.5, 130.0, 127.7, 126.9, 126.3, 125.0, 124.6, 123.5, 118.7, 114.6; HRMS (ESI): m/z calcd for C$_{17}$H$_{11}$N$_3$NaO$_3$ [(M + Na)$^+$] 328.0693, found 328.0691; anal. calcd for C$_{17}$H$_{11}$N$_3$O$_3$ (305.08): C, 66.88; H, 3.63; N, 13.76%. Found: C, 66.83; H, 3.58; N, 13.72%.

General procedure for the synthesis of heteroaryl napthyl ketones 7 and 8. A mixture of formylchromone **1** (1 mmol, 224 g) and thiosemicarbazide or 2-aminothiophenol (1 mmol) in absolute ethanol (20 mL) was refluxed for 15 min. The precipitated solid during reflux was collected by filtration and crystallized from DMF/EtOH to give pure products **7** and **8**.

6-(1-Hydroxy-2-naphthoyl)-3-thioxo-3,4-dihydro-2H-1,2,4-triazepine (7). Yield (291 mg, 98%); gray crystals; m.p. = 338–

339 °C; IR (KBr, ν/cm^{-1}) = 3410 (OH), 3212 (NH), 3156 (NH), 1639 (CO$_{Ketone}$); ^{1}H NMR (500 MHz, DMSO-d_6) δ (ppm): 7.84–7.78 (m, 2H, naphthyl–H), 7.96 (d, 1H, naphthyl–H, J = 8.75 Hz), 8.03 (d, 1H, naphthyl–H, J = 8.75 Hz), 8.12 (d, 1H, naphthyl–H, J = 7.70 Hz), 8.16 (s, 1H, triazepine–H), 8.22 (s, 1H, OH or NH, exchangeable with D$_2$O), 8.29 (s, 1H, triazepine–H), 8.48 (d, 1H, naphthyl–H, J = 7.70 Hz), 9.36 (s, 1H, OH or NH, exchangeable with D$_2$O), 11.60 (s, 1H, OH or NH, exchangeable with D$_2$O); ^{13}C NMR (150 MHz, DMSO-d_6) δ (ppm): 178.1, 174.5, 154.4, 153.0, 135.4, 133.9, 129.8, 128.3, 127.9, 125.9, 123.3, 121.9, 120.1, 119.75, 119.67; EI-MS m/z (%): 94.49 (60.60%), 122.09 (100.00), 169.21 (51.35%), 174.03 (46.47%), 279.15 (55.43%), 290.87 (59.44%), 297.90 (19.90%), 299.08 (12.28%); HRMS (ESI): m/z calcd for C$_{15}$H$_{11}$N$_3$NaO$_2$S [(M + Na)$^+$] 320.0464, found 320.0452; anal. calcd for C$_{15}$H$_{11}$N$_3$O$_2$S (297.06): C, 60.59; H, 3.73; N, 14.13; S, 10.78%. Found: C, 60.63; H, 3.76; N, 14.05; S, 10.72%.

3-(1-Hydroxy-2-naphthoyl)benzo[b][1,4]thiazepine (8). Yield (325 mg, 98%); orange crystals; m.p. = 220–221 °C; IR (KBr, ν/cm^{-1}) = 3450–3325 (OH), 1660 (CO$_{Ketone}$), 1626 (C=N); ^{1}H NMR (400 MHz, CDCl$_3$): δ (ppm) 7.37 (d, 1H, Ar–H, J = 10.80 Hz), 7.64–7.55 (m, 3H, Ar–H), 7.74 (s, 1H, thiazepine–H), 7.81 (d, 1H, Ar–H, J = 10.00 Hz), 7.91 (dd, 2H, Ar–H, J = 11.00, 11.60 Hz), 8.05 (d, 1H, Ar–H, J = 11.00 Hz), 8.16 (d, 1H, Ar–H, J = 10.50 Hz), 8.19 (s, 1H, thiazepine–H), 8.45 (d, 1H, Ar–H, J = 10.00 Hz), 12.50 (s, 1H, OH, exchangeable with D$_2$O); HRMS (ESI): m/z calcd for C$_{20}$H$_{13}$NNaO$_2$S [(M + Na)$^+$] 354.0559, found 354.0575; anal. calcd for C$_{20}$H$_{13}$NO$_2$S (331.07): C, 72.49; H, 3.95; N, 4.23, S, 9.67%. Found: C, 72.42; H, 3.99; N, 4.31, S, 9.65%.

Synthesis of 11-ethoxy-2,11-dihydrobenzo[7,8]chromeno[4,3-c]pyrazole (10). A mixture of formylchromone **1** (1 mmol, 224 mg) and hydrazine hydrate (1 mmol) in absolute ethanol (5 mL) was stirred for 30 min. After cooling to room temperature, the formed precipitate was collected by filtration, washed with dry ethanol, dried, and crystallized from methanol to give product **5**. Yield (231 mg, 97%); Pale yellow crystals; m.p. = 210–211 °C; IR (KBr, ν/cm^{-1}) = 3164 (NH), 2967, 2862 (CH$_{Aliphatic}$), 1632 (C=N); ^{1}H-NMR (400 MHz, DMSO-d_6) δ (ppm): 1.06 (t, 3H, CH$_2$CH$_3$, J = 6.80 Hz), 3.45 (q, 2H, CH$_2$CH$_3$, J = 6.80 Hz), 4.39 (br. s, 1H, NH, exchangeable with D$_2$O), 6.94 (s, 1H, H-2$_{Chromene}$), 7.57–7.55 (m, 2H, H-Ar–H), 7.61–7.59 (m, 2H, Ar–H), 7.92 (d, 1H, Ar–H, J = 8.01 Hz), 8.32 (d, 1H, Ar–H, J = 8.01 Hz), 8.66 (brs, 1H, CH$_{Pyrazole}$); ^{13}C NMR (150 MHz, DMSO-d_6) δ (ppm): 154.4, 151.0, 134.3, 127.6, 127.0, 125.5, 125.4, 122.6, 119.3, 114.7, 111.5, 56.1, 18.6; EI-MS m/z (%): 50.92 (46.23%), 58.47 (57.12%), 98.4 (74.18%), 106.85 (70.21%), 195.09 (68.37%), 214.05 (100.00), 238.49 (37.40%); HRMS (ESI): m/z calcd for C$_{16}$H$_{15}$N$_2$O$_2$ [(M + H)$^+$] 267.1128, found 267.11.21; anal. calcd for C$_{16}$H$_{14}$N$_2$O$_2$ (266.11): C, 70.12; H, 5.30; N, 10.52%. Found: C, 70.21; H, 5.36; N, 10.42%.

Synthesis of 3-(1-hydroxy-2-naphthoyl)-4-(hydrazineylidene methyl)-1H-pyrazole (11). A mixture of formylchromone **1** (1 mmol, 224 mg) and hydrazine hydrate (2 mmol) in absolute ethanol (5 mL) was refluxed for 2 h. The reaction mixture was left to stand overnight, and then the precipitate was purified by column chromatography to afford pure pyrazole **6**. Yield (248 mg, 98%); Deep yellow crystals; m.p. = 224–225 °C; IR (KBr, ν/cm^{-1}) = 3651–3420 (OH, NH$_2$), 3259 (NH), 1616 (C=N), 1574 (C=C); ^{1}H-NMR (400 MHz, DMSO-d_6): δ (ppm) 7.19 (br. s, 2H, NH$_2$), 7.75–7.54 (m, 5H, Ar–H, CH=N), 7.92 (d, 1H, Ar–H, J = 8.00 Hz), 8.32 (d, 1H, Ar–H, J = 8.00 Hz), 8.67 (brs, 1H, CH$_{Pyrazole}$), 10.61 (s, 1H, OH or NH), 13.6 (s, 1H, OH or NH); ^{13}C NMR (100 MHz, DMSO-d_6): δ (ppm) 115.10, 116.63, 119.81, 123.08, 125.79, 126.02, 127.46, 127.84, 128.06, 128.69, 129.38, 134.73, 151.36, 154.84; EI-MS m/z (%): 77.24 (72.11%), 122.06 (82.14%), 151.26 (100.00%), 152.19 (62.05%), 166.96 (48.52%), 202.12 (56.76%), 216.92 (57.41%), 252.00 (11.34%); HRMS (ESI): m/z calcd for C$_{14}$H$_{12}$N$_4$NaO [(M + Na)$^+$] 275.0903, found 275.0901; anal. calcd for C$_{14}$H$_{12}$N$_4$O (252.10): C, 66.65; H, 4.79; N, 22.21%. Found: C, 70.53; H, 4.37; N, 11.72%.

General procedure for the synthesis of Schiff bases 12a,b. To a hot solution of formylchromone **1** (1 mmol, 224 mg) in absolute methanol (15 mL), 4-aminoantipyrine or 2-benzothiazolamine (1 mmol) was added followed by reflux for 30 min. The formed precipitate was collected by filtration and washed by methanol to give pure Schiff bases **12a,b**.

1,5-Dimethyl-4-(((4-oxo-4H-benzo[h]chromen-3-yl)methylene)amino)-2-phenyl-1,2-dihydro-3H-pyrazol-3-one (12a). Yield (402 mg, 98%); yellow crystals; m.p. = 342–343 °C; IR (KBr, ν/cm^{-1}) = 2975, 2916 (CH$_{Aliphatic}$), 1653 (CO), 1622 (CO), 1602 (C=N); ^{1}H NMR (500 MHz, CDCl$_3$) δ (ppm): 2.49 (s, 3H, CH$_3$), 3.15 (s, 3H, NCH$_3$), 7.30 (t, 1H, Ar–H, J = 7.25 Hz), 7.38 (d, 2H, Ar–H, J = 7.55 Hz), 7.45 (dd, 2H, Ar–H, J = 7.25, 7.55 Hz), 7.69–7.63 (m, 2H, Ar–H) 7.76 (d, 1H, Ar–H, J = 8.65 Hz), 7.90 (d, 1H, Ar–H, J = 7.60 Hz), 8.19 (d, 1H, Ar–H, J = 8.65 Hz), 8.46 (d, 1H, Ar–H, J = 7.60 Hz), 8.93 (s, 1H, chromone–H), 9.87 (s, 1H, CH=N); ^{13}C NMR (150 MHz, CDCl$_3$) δ (ppm): 188.8, 175.6, 167.8, 160.3, 159.5, 153.6, 150.7, 135.9, 134.6, 129.3, 129.2, 128.1, 127.2, 127.0, 125.6, 124.5, 124.0, 122.2, 122.1, 121.1, 121.0, 35.8, 10.3; EI-MS m/z (%): 73.13 (50.42%), 77.15 (65.69%), 267.18 (32.21%), 295.22 (58.23%), 336.25 (100.00%), 354.20 (48.79%), 409.02 (3.45%); HRMS (ESI): m/z calcd for C$_{25}$H$_{19}$N$_3$NaO$_3$ [(M + Na)$^+$] 432.1319, found 432.1319; anal. calcd for C$_{25}$H$_{19}$N$_3$O$_3$ (409.14): C, 73.34; H, 4.68; N, 10.26%. Found: C, 73.32; H, 4.71; N, 10.31%.

3-((Benzo[d]thiazol-2-ylimino)methyl)-4H-benzo[h]chromen-4-one (12b). Yield (348 mg, 98%); yellow crystals; m.p. = 236–237 °C; IR (KBr, ν/cm^{-1}) = 1652 (CO), 1612 (CN); ^{1}H-NMR (500 MHz, DMSO-d_6) δ (ppm): 7.29 (dd, 1H, Ar–H, J = 1.05, 7.35 Hz), 7.43 (dd, 1H, Ar–H, J = 2.35, 9.75 Hz), 7.65–7.62 (m, 2H, Ar–H), 7.76 (d, 1H, Ar–H, J = 7.95 Hz), 7.73 (dd, 1H, Ar–H, J = 7.45, 8.55 Hz), 7.87 (dd, 1H, Ar–H, J = 1.35, 7.20 Hz), 7.97 (m, 2H, Ar–H), 8.33 (d, 1H, Ar–H, J = 8.30 Hz), 9.09 (s, 1H, chromone–H), 10.20 (s, 1H, CH=N); HRMS (ESI): m/z calcd for C$_{21}$H$_{12}$N$_2$NaO$_2$S [(M + Na)$^+$] 379.0512, found 379.0506; anal. calcd for C$_{21}$H$_{12}$N$_2$O$_2$S (356.06): C, 70.77; H, 3.39; N, 7.86; S, 9.00%. Found: C, 70.72; H, 3.41; N, 7.81; S, 9.07%.

Biological evaluation

Antitumor activity

The cells of human liver carcinoma (HepG-2), and human breast adenocarcinoma (MCF-7) were purchased from the American Type Culture Collection (Rockville, MD). All cells were maintained in a DMEM medium, which was supplemented with 10% of heat-inactivated fetal bovine serum (FBS), 100 U ml^{-1} of each of penicillin and streptomycin. The cells were grown at

37 °C in a humidified atmosphere of 5% CO_2. The cytotoxicity activities on the HepG-2, and MCF-7 human cancer cell lines were estimated, employing the 3-(4,5-dimethyl-2-thiazolyl)-2,5-diphenyl-2H-tetrazolium bromide (MTT) assay, which was grounded on the reduction of the tetrazolium salt by the mitochondrial dehydrogenases in viable cells.[30] The cells were dispensed in a 96 well sterile microplate (3×10^4 cells per well), followed by their incubation at 37 °C with a series of different concentrations of 10 μL of each compound or Doxorubicin® (positive control, in DMSO) for 48 h in a serum-free medium prior to the MTT assay. Subsequently, the media were carefully removed, 40 μL of MTT (2.5 mg mL^{-1}) was added to each well, and then incubated for an additional 4 h. The purple formazan dye crystals were solubilized by the addition of 200 μL of DMSO. The absorbance was measured at 570 nm applying a SpectraMax® Paradigm® Multi-Mode microplate reader. The relative cell viability was expressed as the mean percentage of viable cells relative to the untreated control cells. All experiments were conducted in triplicate and were repeated on three different days. All the values were represented as mean ± SD. The IC$_{50}$s were determined by the SPSS probit analysis software program (SPSS Inc., Chicago, IL).

Anti-inflammatory activity

The ability of the synthesized compounds to inhibit ovine COX-1 and COX-2 (IC$_{50}$ values) was determined using an enzyme immunoassay (EIA) kit (Catalog number 560101, Cayman Chemical, Ann Arbor, MI, USA). Briefly, to a series of supplied reaction buffer, solutions (960 mL, 0.1 M Tris HCl pH 8.0 containing 5 mM EDTA and 2 mM phenol) with either COX-1 or COX-2 (10 mL) enzyme in the presence of heme (10 mL) were added 10 mL of various concentrations of test drug solutions (1000–0.49 μg mL^{-1} in a final volume of 1 mL). These solutions were incubated for 5 min at 37 °C after which 10 mL of AA (100 mM) solution were added and the COX reaction was stopped by the addition of 50 mL of 1 M HCl after 2 min. This assay is based on the competition between PGs and a PG-acetylcholinesterase conjugate (PG tracer) for a limited amount of PG antiserum. The amount of PG tracer that can bind to the PG antiserum is inversely proportional to the concentration of PGs in the wells since the concentration of PG tracer is held constant while the concentration of PGs varies. This antibody ePG complex binds to a mouse anti-rabbit monoclonal antibody that had been previously attached to the well. The plate is washed to remove any unbound reagents and then Ellman's reagent, which contains the substrate to acetylcholine esterase, is added to the well. The product of this enzymatic reaction produces a distinct yellow color that absorbs at 406 nm. IC$_{50}$ value is the compound concentration required to produce 50% inhibition of COX-1 or COX-2 for means of two determinations using an ovine COX-1/COX-2 assay kit (USA) (triplicate determinations). Selectivity index (COX-1 IC$_{50}$/COX-2 IC$_{50}$).

Antituberculosis activity

The *Mycobacterium tuberculosis* (RCMB 010126) strain was provided from the Regional Center for Mycology and Biotechnology (RCMB), Al-Azhar University (Cairo, Egypt). Antimycobacterial activity of the synthesized compounds was performed using the microplate Alamar blue assay (MABA) which was performed in black, clear-bottomed, 96 well microplates to minimize background effects.[31] Outer perimeter wells were filled with sterile water to prevent dehydration in experimental wells. Initial compounds dilutions were prepared in dimethyl sulfoxide and subsequent twofold dilutions were performed in the microplates. 0.1 mL of 105 CFU mL^{-1} *Mycobacterium tuberculosis* inoculum was added to wells, additional control wells consisted of bacteria only (B). Isoniazid was used as a reference drug. Plates were incubated at 37 °C. Starting at day 4 of incubation, 20 μL of alamar Blue solution (Alamar Biosciences/Accumed, Westlake, OH, USA) and 12.5 μL of 20% Tween 80 were added to the entire plate. Plates were then incubated at 37 °C, and results were recorded at 24 h post-reagent addition at 590 nm. Percent inhibition was defined as [1 − (mean of test well/mean of B wells) × 100]. Visual MICs were defined as the lowest concentration of drug that prevented a color change.

Computational analysis

Molecular docking

To predict the inhibition mechanisms and the most suitable targets for the synthesized compounds, several biological targets related to anticancer, anti-inflammatory, and antituberculosis activities were screened. The crystal structures Human DEAD-box RNA helicase DDX3X (PDB 2I4I) and Human topoisomerase II (PDG 5GWK) as cancer targets; COX-1 (PDB 1EGQ) and COX-2 (PDB 4PH9) as anti-inflammatory targets; *M. tuberculosis* InhA enzyme (PDB 4DRE) as tuberculosis target were selected and fetched from Protein Data Bank (www.rcsb.org/pdb). Chemical structures of ligands were drawn into Marvin Sketch (ChemAxon) and the most energetically favored conformer was saved as (*.sdf) file format for docking. Molecular AutoDock 4.2 (MGL tools-1.5.6) docking protocol was performed using PYRX software.[32] Prior to the semi-flexible docking, the target proteins were cleaned up by removing water molecules and adding hydrogen atoms to obtain correct ionization and tautomeric states of amino acid residues. All rotatable bonds could rotate during the docking process, and protein-ligand interactions were saved in the PDBQT format suitable for calculating binding energy. The structure of ligand and its complexes were transformed into PDB file format using PYMOL software (Version 2.2.3).

Conflicts of interest

The authors declare no competing financial interests.

Acknowledgements

References

1 S. Makar, T. Saha and S. K. Singh, *Eur. J. Med. Chem.*, 2019, **161**, 252–276.

2 (*a*) S. I. El-Desoky, E. M. Keshk, A. A. El-Sawi, M. A. Abozeid, L. A. Abouzeid and A. H. Abdel-Rahman, *Saudi Pharm. J.*, 2018, **26**, 852–859; (*b*) M. A. Abozeid, M. R. El-Kholany, A. H. Abdel-Rahman and S. I. El-Desoky, *Int. J. Mod. Org. Chem.*, 2018, **5**, 1–11; (*c*) M. A. Abozeid, M. R. El-Kholany, L. A. Abouzeid, A. H. Abdel-Rahman and S. I. El-Desoky, *J. Heterocycl. Chem.*, 2019, **56**, 2922–2933; (*d*) S. I. El-Desoky, A. A. El-Sawi, M. A. Abozeid, M. Abdelmoteleb, M. Shaaban, E. M. Keshk and A. H. Abdel-Rahman, *Med. Chem. Res.*, 2019, **28**, 1601–1617; (*e*) M. A. Abozeid, A. A. El-Sawi, M. R. Elmorsy, M. Abdelmoteleb, A. H. Abdel-Rahman and S. I. El-Desoky, *RSC Adv.*, 2019, **9**, 27996–28005.

3 (*a*) S. Valente, D. Trisciuoglio, T. De Luca, A. Nebbioso, D. Labella, A. Lenoci, C. Bigogno, G. Dondio, M. Miceli and G. Brosch, *J. Med. Chem.*, 2014, **57**, 6259–6265; (*b*) C. Abate, M. Niso, E. Lacivita, P. D. Mosier, A. Toscano and R. Perrone, *J. Med. Chem.*, 2011, **54**, 1022–1032.

4 R. Perrone, F. Doria, E. Butovskaya, I. Frasson, S. Botti, M. Scalabrin, S. Lago, V. Grande, M. Nadai, M. Freccero and S. N. Richter, *J. Med. Chem.*, 2015, **58**, 9639–9652.

5 Z. Özdemir, S. Sari, A. Karakurt and S. Dalkara, *Drug Dev. Res.*, 2019, **80**, 269–280.

6 S. K. Das, G. Panda, V. Chaturvedi, Y. S. Manju, A. K. Gaikwad and S. Sinha, *Bioorg. Med. Chem. Lett.*, 2007, **17**, 5586–5589.

7 E. A. Boyle, P. C. Freemanm, F. R. Mangan and M. J. Thomson, *J. Pharm. Pharmacol.*, 1982, **34**, 562–569.

8 T. A. Unzner, A. S. Grossmann and T. Magauer, *Angew. Chem., Int. Ed.*, 2016, **55**, 9763–9767.

9 D. Quan, G. Nagalingam, R. Payne and J. A. Triccas, *Int. J. Infect. Dis.*, 2017, **56**, 212–220.

10 H.-J. Zhang, E. Rumschlag-Booms, Y.-F. Guan, D.-Y. Wang, K.-L. Liu, W.-F. Li, V. H. Nguyen, N. M. Cuong, D. D. Soejarto, H. H. S. Fong and L. Rong, *J. Nat. Prod.*, 2017, **80**, 1798–1807.

11 R. F. Luduena, M. C. Roach and P. Horowitz, *Biochim. Biophys. Acta, Protein Struct. Mol. Enzymol.*, 1986, **873**, 143–146.

12 W. Molee, A. Phanumartwiwath, C. Kesornpun, S. Sureram, N. Ngamrojanavanich, K. Ingkaninan, C. Mahidol, S. Ruchirawat and P. Kittakoop, *Chem. Biodiversity*, 2018, **15**, e1700537.

13 F.-Y. Chang, J. E. Peacock Jr, D. M. Musher, P. Triplett, B. B. MacDonald, J. M. Mylotte, A. O'Donnell, M. M. Wagener and L. Y. Victor, *Medicine*, 2003, **82**, 333–339.

14 M. V. Worley and S. J. Estrada, Bedaquiline, *Pharmacotherapy*, 2014, **34**, 1187–1197.

15 F. K. Chan, N. S. Abraham, J. M. Scheiman and L. Laine, *Am. J. Gastroenterol.*, 2008, **103**, 2908–2918.

16 D. W. Robertson, J. H. Krushinski, E. Beedle, J. D. Leander, D. T. Wong and R. Rathbun, *J. Med. Chem.*, 1986, **29**, 1577–1586.

17 J. Zheng, M. Cho, A. D. Jones and B. D. Hammock, *Chem. Res. Toxicol.*, 1997, **10**, 1008–1014.

18 P. J. Thornalley, M. d. A. Doherty, M. T. Smith, J. V. Bannister and G. M. Cohen, *Chem.-Biol. Interact.*, 1984, **48**, 195–206.

19 P. Jia, C. Dai, P. Cao, D. Sun, R. Ouyang and Y. Miao, *RSC Adv.*, 2020, **10**, 7740–7750.

20 M. Decker, *Design of hybrid molecules for drug development*, Elsevier, Amsterdam, 2017.

21 S. V. Kumar, S. Muthusubramanian and S. Perumal, *Org. Prep. Proced. Int.*, 2019, **51**, 1–89.

22 (*a*) K. M. Elattar, M. A. Abozeid, I. A. Mousa and A. El-Mekabaty, *RSC Adv.*, 2015, **5**, 106710–106753; (*b*) K. A. M. El-Bayouki, *J. Sulphur Chem.*, 2011, **32**, 623–690.

23 X.-J. Huang, Y. Tao, Y.-K. Li, X.-Y. Wu and F. Sha, *Tetrahedron*, 2016, **72**, 8565–8577.

24 (*a*) W. Ried and B. Schleimer, *Angew. Chem.*, 1958, **70**, 164; (*b*) N. Y. Gorobets, B. H. Yousefi, F. Belaj and C. O. Kappe, *Tetrahedron*, 2004, **60**, 8633–8644; (*c*) S. M. Gomha, K. D. Khalil, A. M. El-Zanaty and S. M. Riyadh, *Heterocycles*, 2013, **87**, 1109–1120.

25 S. M. Gomha and K. D. Khalil, *Molecules*, 2012, **17**, 9335–9347.

26 O. Ahmed, V. Cherkadu, P. K. Kalavagunta and J. Shang, *RSC Adv.*, 2019, **9**, 20573–20581.

27 K. T. Savjani, A. K. Gajjar and J. K. Savjani, *ISRN Pharm.*, 2012, **2012**, 195727.

28 Y. C. Martin, *J. Med. Chem.*, 2005, **48**, 3164–3170.

29 N. Mohsin and M. Irfan, *Med. Chem. Res.*, 2020, **29**, 809–830.

30 (*a*) A. F. Kassem, I. F. Nassar, M. T. Abdel-Aal, H. M. Awad and W. A. El-Sayed, *Chem. Pharm. Bull.*, 2019, **67**, 888–895; (*b*) F. M. Alminderej, H. H. Elganzory, M. N. El-Bayaa, H. M. Awad and W. A. El-Sayed, *Molecules*, 2019, **24**, 3738; (*c*) M. E. Haiba, E. S. Al- Abdullah, N. S. Ahmed, H. A. Ghabbour and H. M. Awad, *J. Mol. Struct.*, 2019, **1195**, 702–711.

31 (*a*) M. A. Abdelrahman, I. Salama, M. S. Gomaa, M. M. Elaasser, M. M. Abdel-Aziz and D. H. Soliman, *Eur. J. Med. Chem.*, 2017, **138**, 698–714; (*b*) M. M. Ghorab, M. S. A. El-Gaby, A. M. Soliman, M. S. Alsaid, M. M. Abdel-Aziz and M. M. Elaasser, *Chem. Cent. J.*, 2017, **11**, 42.

32 O. Trott, A. J. Olson and J. Comput, *Chem*, 2010, **31**, 455–461.